Zeitschrift für Physikalische Chemie, **215**, 2, 183–195 (2001)

Quantum Yields for the Photodissociation of Iodine in Compressed Liquids and Supercritical Fluids

By D. Schwarzer*, J. Schroeder and C. Schröder

Max-Planck-Institut für Biophysikalische Chemie, Am Faßberg, D-37077 Göttingen, Germany

Dedicated to Prof. Dr. Dr. h.c. mult. Jürgen Troe on the occasion of his 60th birthday

(Received July 28, 2000; accepted August 15, 2000)

Photolytic Cage Effect

Quantum yields of photodissociation were determined for iodine in compressed liquid *n*-alkanes and supercritical CO_2 and xenon after laser excitation at 532 nm. The quantum yield decreases nearly linearly with increasing density. No cluster effects at low density were observed at this excitation energy. Our results are compared with molecular dynamics simulations and point at the importance of kinematic processes involved in the recombination dynamics of iodine.

1. Introduction

The photodissociation and recombination of iodine is one of the most extensively studied chemical reactions in liquids and, therefore, served as a model system for understanding various aspects of condensed phase reaction dynamics. The interest goes back to Franck and Rabinowitch proposing the possibility that after photoexcitation separating iodine atoms could be trapped in a solvent cage reducing the dissociation quantum yield with respect to the gas phase [1]. Subsequent quantitative investigations of the cage effect by Noyes were aimed at understanding the dependence of iodine dissociation quantum yields on the wavelength of the excitation light and solvent viscosity [2–4]. In systematic studies over wide density ranges Troe and co-workers [5, 6] and van den Bergh and co-workers [7–9] found quantum yields smaller than unity at surprisingly low gas pressures, namely, one or two orders of magnitude below liquid densities. Similar results were obtained with excitation at 694 nm

* Corresponding author. E-mail: dschwar@gwdg.de

and 581 nm, i.e. about 2000 cm^{-1} and 4800 cm^{-1} above the dissociation limit of ground state iodine, respectively. The observed drop in quantum yield was explained by a cluster mechanism proposing the formation of iodine-solvent complexes which after laser excitation fragment and thereby dissipate the excess energy [10, 11].

In liquids at high pressures the quantum yield ϕ_{diss} was found [10, 12] to steeply decrease as

$$\phi_{diss} \propto \eta^{-2}, \tag{1}$$

where η is the solvent viscosity. The latter observation was explained [10, 11] with a diffusion model including an energy relaxation rate constant for the geminately recombined iodine atoms which is inversely proportional to the solvent self diffusion coefficient D. This model suggests that the effective collision frequency Z for vibrational energy relaxation in dense media increases as

$$Z \propto D^{-1}. \tag{2}$$

A detailed microscopic picture of the photodissociation and geminate recombination of iodine bases on picosecond experiments which are available since the mid 1980s (see review [13] and references cited therein). According to these and later studies [14–16] the dynamics is characterised by a variety

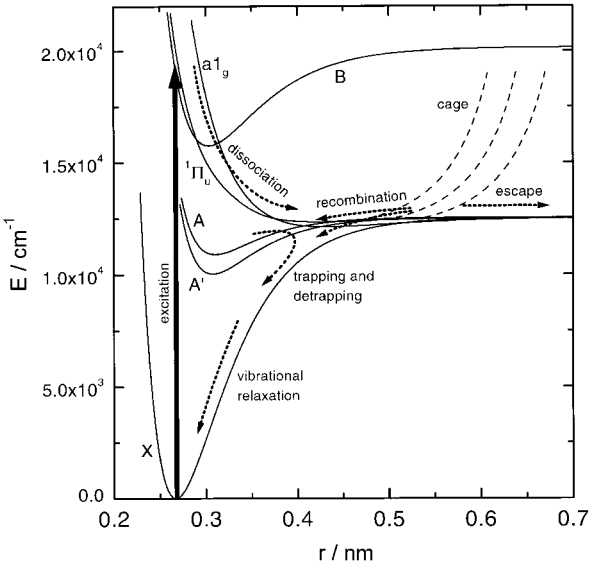

Fig. 1. Photodissociation and recombination of iodine in solution (adapted from [13]).

of competing processes summarised in Fig. 1. After light absorption in the range 450–600 nm the dissociative $B''\,1_u(^1\Pi)$ or predissociative $B\,0_u^+(^3\Pi)$ electronic state is populated causing the iodine atoms to separate on repulsive potentials. A fraction of atoms collide with surrounding solvent particles and recombine geminately in the cage. Partially they get trapped in weakly bound $A\,1_u(^3\Pi)$ and $A'\,2_u(^3\Pi)$ electronic states from which they can relax to the $X\,0_g^+(^1\Sigma^+)$ ground state by radiative or nonradiative transitions. Partially they immediately recombine to the ground state where the iodine molecules are stabilised by vibrational energy relaxation. A fraction of separating atoms succeeds to escape from the solvent cage. These atoms can still recombine geminately within several tens of picoseconds or separate by diffusion and finally nongeminately recombine on a microsecond time scale.

The experimental investigations were accompanied by extensive theoretical studies which in the past often were based on Monte Carlo or classical molecular dynamics (MD) simulations [17–19]. Recently, even the complicated curve crossing problem involved in the recombination process was dealt with in coupled quantum-classical MD simulations by taking into account nonadiabatic transitions among 23 Hund's case (c) covalent molecular states [20].

Most computer simulations and time resolved experimental investigations suggest that the quantum yield for dissociation is mainly determined by the primary in-cage recombination. The partitioning between cage escape and recombination, however, is very fast (1–2 ps), i.e., this process is dominated by highly energetic, nonthermal collisions emphasizing that diffusive models of geminate recombination are inappropriate. On the other hand the interpretation of photodissociation quantum yield measurements of iodine [10] and bromine [21] just bases on such models. Furthermore, an energy relaxation rate constant was deduced from these quantum yield measurements suggesting that the collision frequency Z in dense media is proportional to D^{-1}, see Eq. (2). Recent experiments on the density dependence of the vibrational energy relaxation rate of highly excited azulene, however, clearly show an increase of Z with the local solvent density in the immediate surrounding of the solute [22, 23] which is much weaker than expressed by Eq. (2).

Even more puzzling is the drop of the iodine photodissociation quantum yields observed at relatively low densities. The interpretation that this effect is caused by cluster formation [10] seemed to be supported by experiments with I_2-Ar van der Waals complexes formed in supersonic molecular beams [24, 25]. In these experiments, photoexciting the region 0–1400 cm^{-1} above the $B\,0_u^+(^3\Pi)$ state dissociation limit of the bare I_2 molecule, fluorescence from a vibrational distribution within the B state was observed. The implication of these experiments is that fragmentation of the van der Waals complex can leave the I_2 molecule below its dissociation limit while the excess energy is deposited in the I_2-solvent relative translational motion. For a long time it was unclear what dynamical mechanism was responsible for

this so-called one-atom cage effect, since over the years many of the noble gas-I_2, -Br_2 and -Cl_2 structures were found to be of triangular (or T-shaped) geometry (see [26] and references cited therein) which make a kinematic interpretation of the phenomenon difficult. Attempts to interpret the I_2-Ar data using triangular geometry by means of non-adiabatic models were made [27], but now it is known that the one-atom cage effect is due to a linear isomer [28]. Recent wave packet and quasiclassical trajectory calculations confirm that the I_2-Ar photodissociation-recombination can be explained as a purely kinematic process on the B state electronic surface of the collinear cluster [29, 30].

In contrast to these molecular beam experiments, the low density quantum yield measurements of Troe and co-workers on iodine were performed in the bulk at $T \geq 314$ K [5, 6]. Although it is feasible that a sufficient number of van der Waals complexes is present under conditions where the cluster effect was observed [31], the probability that they appear in a linear geometry is very unlikely due to thermal excitation of the clusters. Furthermore, the excess energy in these studies was considerably higher than in the molecular beam experiments where the one-atom cage effect was observed. This brings us back to the problem to imagine a mechanism which accounts for the photoabsorptive dissociation of the complex into a solvent fragment and a vibrationally excited iodine molecule in the bound A, A′, or ground state (attempts into this direction have been made by Dardi and Dahler [32]).

In order to elucidate the reasons for the discrepancies discussed above, we re-determined iodine dissociation quantum yields over wide pressure ranges after photoexcitation at 532 nm. We will show that in contrast to earlier studies the quantum yield ϕ_{diss} decreases nearly linearly with density and that at low densities there is no evidence for a cluster effect. Experimental results are in agreement with model calculations basing on MD-simulations.

2. Experimental technique

In our experiments I_2 was photolyzed by nanosecond laser pulses at 532 nm. The quantum yield for I_2 dissociation was measured directly after the laser pulse by monitoring the bleaching of molecular iodine absorption at 514 nm. The experimental setup is shown schematically in Fig. 2. The excitation light source was a frequency doubled Q-switched Nd:YAG laser (Quantel Brillant) operating at a repetition rate of 25 Hz with pulse lengths of 5 ns. An aperture placed in front of the sample cell restricted the diameter of the laser beam to 5.0 mm generating a nearly homogenous circular profile. The pulse energy behind the aperture was typically 6 mJ and passed into the sample cell by means of dielectric mirrors. Laser energies were measured in front of and behind the sample cell by means of a calibrated pyroelectric detector. The sample cell was placed in a dual beam absorption spectrometer. Analysis light at 514 nm

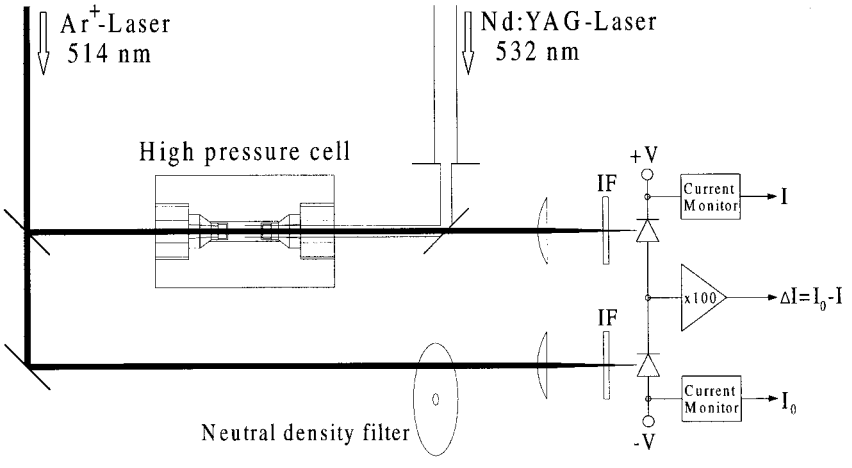

Fig. 2. Experimental setup.

was obtained from a cw argon ion laser (Lexel). 20 mW of the laser light was divided into two paths. The signal beam passed through the sample cell to a photodiode (Hamamatsu, S5972) while the reference beam traveled directly to a second photodiode. A neutral density filter wheel in front of the reference photodiode was used to match the laser intensities. Both photodiodes were protected against excitation light by means of narrow band interference filters and were part of an electronic circuit subtracting their photocurrents $\Delta I(t) = I_0 - I$ as shown in Fig. 2. In this way most of common-mode laser noise was rejected from the signal. The difference signal was amplified and recorded by a digital oscilloscope (Tektronics, TDS 640, 500 MHz). After averaging about 2000 laser excitation pulses changes of the iodine optical density were derived according to $\Delta\mathrm{OD}(t) = \log(I_0/(I_0 - \Delta I(t)))$ were I_0 was determined from the low frequency current monitor of the reference photodiode. The over all time resolution of the absorption spectrometer was 10 ns which is slow enough to fade out geminate recombination and vibrational relaxation dynamics but sufficient to give reliable information about photodissociation quantum yields of iodine.

Experiments in supercritical fluids between 1 and 30 bar were performed in a heatable stainless steel cell with an optical path length of 20 cm. At higher pressures and for liquids a heatable high pressure cell with an optical path length of 22 mm was used. Both cells were equipped with sapphire windows of thickness 7 mm and aperture 5 mm. The windows were held by conical fittings. Temperature was measured with an accuracy of 0.2 K, the precision determining pressures was 1%. I_2 concentrations inside the cell were adjusted to $\leq 10^{-3}$ mol/l and solvents (p.a. grade, J. T. Baker) and gases (Messer–Griesheim) were used without further purification.

3. Results and discussion

3.1 Photolysis quantum yields

In Fig. 3 typical absorption signals of molecular iodine in supercritical xenon at 41 and 1022 bar after excitation with a 5 ns laser pulse at 532 nm are shown. The temperature was 313 K. Assuming that geminate cage recombination, vibrational energy relaxation, and other fast phenomena are complete after 10 ns, iodine photodissociation quantum yields ϕ_{diss} were derived from absorption jumps ΔOD at $t = 0$ and the number of excitation photons absorbed in the sample. The latter was derived from the laser pulse energies in front of and behind the high pressure cell. In the analysis, reflection losses at air-sapphire and sapphire-sample interfaces were taken into account using refractive indices of sapphire of $n = 1.78$ and of the samples as derived from the Lorentz–Lorenz formula. The slow increase of the absorption signals in Fig. 3 at $t > 0$ is due to nongeminate recombination of iodine which at high densities is a diffusion controlled process and well understood [10, 21].

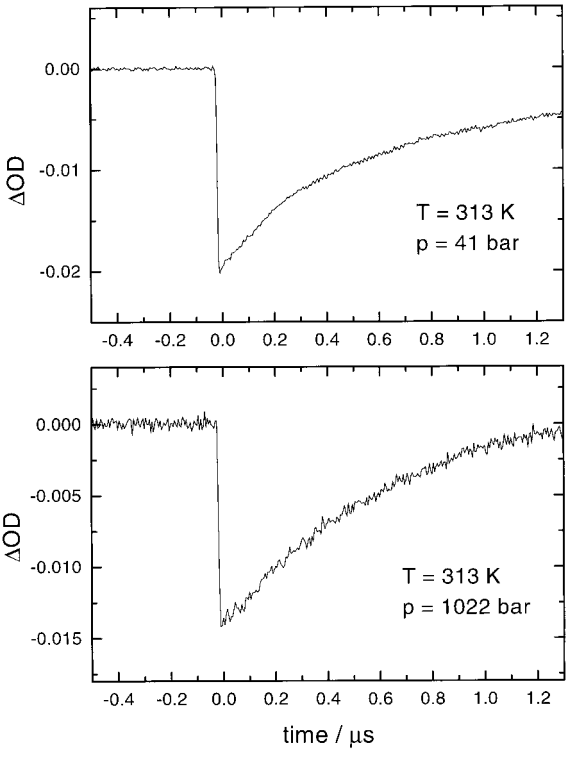

Fig. 3. Recombination of iodine in xenon at 41 and 1022 bar after photodissociation with laser pulses at 532 nm (observation wavelength: 514 nm; $T = 313$ K).

For the calculation of photodissociation quantum yields, absorption coefficients at excitation and observation wavelengths of $\varepsilon_{532} = 888\,\mathrm{l\,mol^{-1}\,cm^{-1}}$ and $\varepsilon_{514} = 898\,\mathrm{l\,mol^{-1}\,cm^{-1}}$, respectively, were used. Since both wavelengths are very close to the centre of the broad I_2 absorption band and this band was shown to hardly shift with pressure, we assumed ε_{532} and ε_{514} to be constant over the whole density range. Then ϕ_{diss} was calculated according to Lambert–Beer's law:

$$\phi_{\mathrm{diss}} = -\Delta\mathrm{OD}(t=0)\frac{\pi r^2 N_{\mathrm{A}}}{\varepsilon_{514} N_{\mathrm{P}}}, \tag{3}$$

where r, N_{P}, and N_{A} are the radius of the excitation laser beam in the sample, the number of absorbed photons, and Avogadro's number, respectively.

Our results for photodissociation quantum yields of iodine in liquid *n*-pentane, *n*-hexane, and *n*-heptane at room temperature are shown in Fig. 4. Within experimental error ϕ_{diss} linearly decreases with density for all liquids as indicated by dashed lines which intersect at $\phi_{\mathrm{diss}}(\varrho = 0) = 1$. For comparison, data from [10, 12] are shown which were obtained in *n*-heptane after laser excitation at 590 nm. These quantum yields are considerably below our results and strongly deviate from a linear density dependence.

In Fig. 5 photodissociation quantum yields for iodine in supercritical CO_2 at 323 K are shown (full squares). At each density several experiments were performed. The error bars indicate the standard deviation of the measured quantum yields. As for the alkanes, ϕ_{diss} decreases nearly linearly with density. A comparison with older data shows strong deviations. At low densities strong cluster effects in CO_2 were found using excitation wavelengths of 694 nm [5]

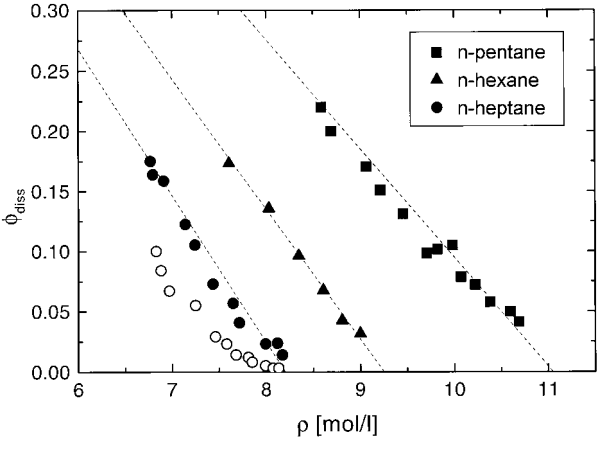

Fig. 4. Photodissociation quantum yields of iodine in compressed liquid *n*-alkanes at 298 K (full symbols: excitation at 532 nm, this work; open circles: excitation at 590 nm, from [10, 12]; dashed lines intercept at $\phi_{\mathrm{diss}}(\varrho = 0) = 1$).

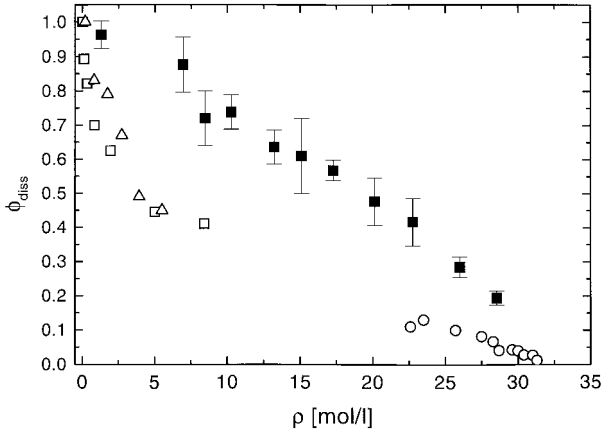

Fig. 5. Photodissociation quantum yields of iodine in CO_2 (■ : $\lambda_{exc} = 532$ nm at 323 K, this work; ○ : $\lambda_{exc} = 590$ nm at 298 K [10]; △ : $\lambda_{exc} = 581$ nm at 330 K [6]; □ : $\lambda_{exc} = 694$ nm at 314 K [5]).

(open squares) and 581 nm [6] (open triangles), respectively. Also at liquid densities, at an excitation wavelength of 590 nm the reported quantum yields were much lower [10] (open circles). In supercritical xenon at 313 K we observed a similar density dependence as for CO_2. As shown in Fig. 6, ϕ_{diss} is monotonously decreasing with density. Note that at low densities no cluster effect can be observed, although xenon is a highly polarizable solvent. Even at the highest densities the photodissociation quantum yield is still around 25%. Slightly higher quantum yields were found in xenon at 323 K by van den Bergh and co-workers [8, 9] after excitation to the A or A′ state at a wavelength of 694 nm (open triangles).

A comparison of iodine photodissociation quantum yields in different solvent is most illuminating. In Fig. 7 all our data of Figs. 4–6 are plotted versus the reduced solvent density $\varrho_r = \varrho/\varrho_c$, where ϱ_c is the critical density of the corresponding solvent. This density scale is a measure of the packing fraction of the respective fluid. As is evident from Fig. 7, all the data nearly fall on a single line, indicating that ϕ_{diss} is mainly proportional to the free space which is available to the iodine atoms when they separate during the dissociation process. The mass of the solvent is of minor importance as was already concluded from early Monte Carlo simulations [17].

3.2 Molecular dynamics simulations

In the following we will compare our results in supercritical xenon with quantum yields from classical molecular dynamics (MD) simulations carried out by standard methods. In order to simplify the calculations we have neglected any curve crossings during the dissociation process of iodine. Although elab-

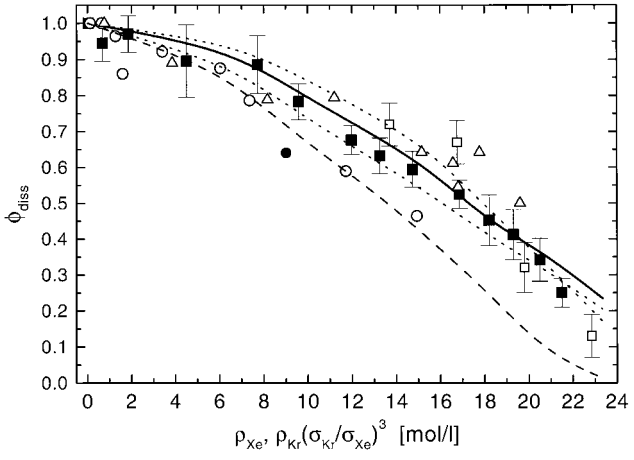

Fig. 6. Photodissociation quantum yields of iodine in xenon (■ : $\lambda_{exc} = 532$ nm at 313 K, this work; △ : $\lambda_{exc} = 694$ nm at 323 K [8, 9]; ○ : in krypton with $\lambda_{exc} = 694$ nm at 298 K (density scaled) [5]). The experimental data are compared with MD simulations of iodine in xenon (——: excitation to the $^1\Pi_u$ state ($R = 0.55$ nm); · · · · · · : excitation to the $^1\Pi_u$ state (upper curve: $R = 0.45$ nm, lower curve: $R = 0.65$ nm); ------ : excitation to the A′ state; □ : excitation to the $^1\Pi_u$ state [19]; ● : excitation in the ground state [18]).

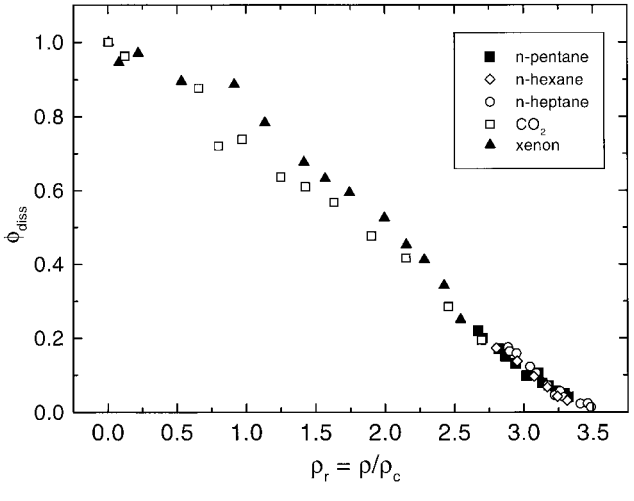

Fig. 7. Photodissociation quantum yields of iodine versus the reduced solvent density (ϱ_c is the critical density of the solvent).

orate methods are available to handle this problem [20, 33] they are still too expensive to calculate trajectories of several tens of picoseconds length necessary for modelling the geminate recombination process. In order to elucidate

the influence of the laser wavelength on ϕ_{diss} we conducted two types of simulations, namely excitation to the repulsive $^1\Pi_u$ state by a 532 nm photon and excitation to the weakly bound A′ state by a 694 nm photon. The model system used in this study consisted of one I_2 molecule immersed in 254 and 498 xenon atoms at low and high (> 12 mol/l) densities, respectively. A cubic simulation box with periodic boundary conditions was used. The simulations were performed in a microcanonical ensemble employing the leap-frog Verlet algorithm. All particles interacted via pairwise additive potentials with a cut-off radius of half the box length. Xenon-xenon and xenon-iodine interactions were treated by Lennard-Jones potentials. For the iodine ground and excited A′ state Morse potentials were used. The repulsive iodine $^1\Pi_u$ state was of the form $c(r/\alpha)^{-9.5}$ [34]. Potential parameters used in this study are listed in Table 1.

The simulations were started on the iodine ground state potential at a specified density from a face centred cubic structure of 256 or 500 particles, two of which were iodine atoms separated by 0.260 nm, and the remaining were xenon atoms. The initial velocities of the particles corresponded to 300 K. After 10 000 integration steps (1 fs step size) with velocity scaling the desired temperature of about 313 K was usually reached. The system was further equilibrated for 100 ps.

Initial conditions for trajectories on the excited surfaces were prepared in accord with the Franck-Condon principle for vertical transitions, i.e. the initial I-I distance $r_{\text{I-I}}$ was derived from $h\nu = V_e(r_{\text{I-I}}) - V_g(r_{\text{I-I}})$, where $h\nu$ is the

Table 1. Potential parameters.

Xe-Xe[1)]	$4\varepsilon[(\sigma/r)^{12} - (\sigma/r)^6]$ $\sigma = 0.4055$ nm $\varepsilon/k_B = 229$ K
I-Xe[1)]	$4\varepsilon[(\sigma/r)^{12} - (\sigma/r)^6]$ $\sigma = 0.394$ nm $\varepsilon/k_B = 328.6$ K
I-I (X-state)[1)]	$D\{\exp[-2\beta(r - r_e)] - 2\exp[-\beta(r - r_e)]\}$ $D/k_B = 18\,044.61$ K $\beta = 18.67$ nm^{-1} $r_e = 0.2668$ nm
I-I (A′-state)[2)]	$D\{\exp[-2\beta(r - r_e)] - 2\exp[-\beta(r - r_e)]\}$ $D/k_B = 3609$ K $\beta = 21.04$ nm^{-1} $r_e = 0.3073$ nm
I-I ($^1\Pi_u$-state)[3)]	$c(r/\alpha)^{-9.5}$ $c/k_B = 1.238 \cdot 10^8$ K $\alpha = 0.1$ nm

[1] [36], [2] [16, 37], [3] [34].

photon energy and V_e and V_g are potential energies of the excited and ground state, respectively. To reach these conditions, trajectories on the ground state were simulated for random times between 5 and 10 ps and continued until the desired value of $r_{I\text{-}I}$ was approached. In this way for each density a pool of 500 starting configurations and velocities were generated which subsequently were propagated for 100 ps on the excited states. During the simulation the I-I distance $r_{I\text{-}I}(t)$ was recorded.

For the repulsive $^1\Pi_u$ state the resulting trajectories were analysed in the following way. A distance R in the range 0.45–0.65 nm where the potential curves of Fig. 1 converge was defined at which the separating iodine atoms are assumed to return to the ground state surface. Once $r_{I\text{-}I}(t)$ exceeded R and subsequently fell below this distance the iodine atoms were counted as recombined. This seems to be a crude simplification of the recombination dynamics, because the iodine atoms in principle can approach each other on a repulsive potential such that after some time they will separate again. Furthermore, even if the iodine atoms remain on the attractive surface, vibrational energy relaxation has to occur to stabilise the I_2 product. At low densities the probability for stabilisation during an encounter is not necessarily one. Both deficiencies of the model would increase the photodissociation quantum yield. Therefore, if they play a role, from our calculations we get lower limits of ϕ_{diss}. In Fig. 8 time dependent photodissociation quantum yields derived from this analysis with $R = 0.55$ nm are shown for various densities. The characteristic time scale for recombination is picoseconds to tens of picoseconds in agreement with earlier calculations [17–19, 35] and time resolved experiments [13, 15]. The quantum yields at the end of the calculations (at $t = 100$ ps) on the repulsive $^1\Pi_u$ state are shown in Fig. 6 and compared with our experimental values and data from

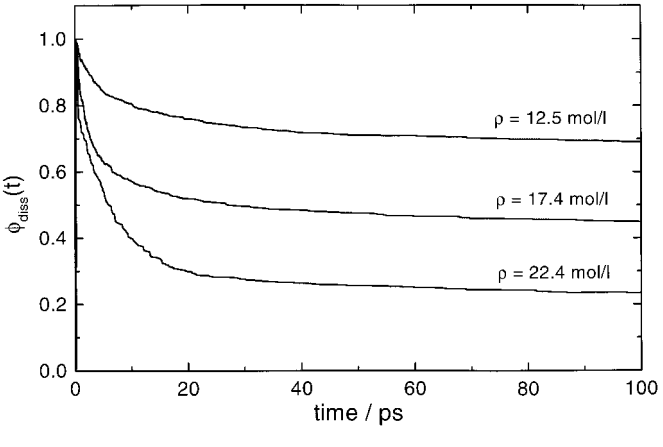

Fig. 8. Time dependent photodissociation quantum yields of iodine in xenon at various densities (MD simulations, excitation to the $^1\Pi_u$ state with $R = 0.55$ nm).

earlier MD-simulations in xenon at 280 K [19]. General agreement is very good. Our simulation results are quite insensitive to the actual choice of R: the full line is obtained with $R = 0.55$ nm, upper and lower dotted lines indicate quantum yields with $R = 0.45$ nm and $R = 0.65$ nm, respectively.

After exciting iodine to the A′ state, the separating atoms do not need to reach the ground state surface to recombine. Instead, due to collisions with xenon atoms, the I_2 molecule can be trapped directly in the attractive well of the A′ potential of 3609 K depth. In our MD simulations the photodissociation quantum yield after excitation to the A′ state was derived from the number of trajectories for which after 100 ps the distance $r_{\text{I-I}}$ was above 0.6 nm relative to the total number of trajectories. The corresponding density dependence of ϕ_{diss} is shown in Fig. 6 by a dashed line. The results are in agreement with classical trajectory simulations on the I_2 ground state surface in the presence of 22 rare gas atoms using 694 nm excitation as well [18] (full circle), whereas the experimental data of van den Bergh et al. seem to high. In Fig. 6 also experimental results for ϕ_{diss} obtained in krypton at 298 K using 694 nm excitation [5] are presented (open circles). To account for the smaller Lennard-Jones diameter of krypton ($\sigma_{\text{Kr}} = 0.366$ nm) with respect to xenon ($\sigma_{\text{Xe}} = 0.4055$ nm), krypton densities were multiplied by a factor $(\sigma_{\text{Kr}}/\sigma_{\text{Xe}})^3$. The agreement with our calculations is excellent supporting the implication of Fig. 7 that ϕ_{diss} is mainly determined by the free space available to the separating iodine atoms rather than the mass of the solvent particles.

Our simulations show that excitation to the A′ state leads to smaller quantum yields than excitation to the repulsive $^1\Pi_u$ state. The reason for this is that on the $^1\Pi_u$ state the I_2 population first has to reach distances where surface hopping to the ground state can occur. At these distances the attractive forces supporting recombination are weak (in our calculations they were essentially zero). In contrast, on the A′ state recombination appears to happen already at the repulsive limb of the potential. This effect is most pronounced at high densities were most trajectories on the A′ potential are characterised by strongly damped oscillations from the Franck-Condon region to the potential well.

4. Conclusions

In the present study we investigated the geminate recombination dynamics of iodine by determining photodissociation quantum yields ϕ_{diss} after laser excitation at 532 nm in compressed liquid *n*-alkanes and supercritical fluids CO_2 and xenon. For all solvents ϕ_{diss} was found to decay nearly linearly with increasing density. A plot of ϕ_{diss} versus the reduced density shows that the quantum yield is independent of the nature of the solvent but mainly determined by the free space available to the separating iodine atoms during the dissociation process. Our results are supported by molecular dynamics simulations and clearly show that the geminate recombination of iodine can be understood in terms of a purely kinematic effect.

Acknowledgement

The authors wish to thank Professor Jürgen Troe for continued support.

References

1. J. Frank and E. Rabinowitch, Trans. Faraday Soc. **30** (1934) 120.
2. F. W. Lampe and R. M. Noyes, J. Am. Chem. Soc. **76** (1954) 2140.
3. D. Booth and R. M. Hoyes, J. Am. Chem. Soc. **82** (1960) 1868.
4. L. F. Meadows and R. M. Noyes, J. Am. Chem. Soc. **82** (1960) 1872.
5. K. Luther, J. Troe, Chem. Phys. Lett. **24** (1974) 85.
6. H. Hippler, K. Luther, M. Maier, J. Schroeder and J. Troe, *Laser Induced Processes in Molecules*, Springer, Heidelberg (1979) 286.
7. C. Dupuy and H. van den Bergh, Chem. Phys. Lett. **57** (1978) 348.
8. J. M. Zellweger and H. van den Bergh, J. Chem. Phys. **72** (1980) 5405.
9. J. C. Dutoit, J. M. Zellweger and H. van den Bergh, J. Chem. Phys. **78** (1983) 1825.
10. B. Otto, J. Schroeder and J. Troe, J. Chem. Phys. **81** (1984) 202.
11. J. Schroeder and J. Troe, Ann. Rev. Phys. Chem. **38** (1987) 163.
12. K. Luther, J. Schroeder, J. Troe and U. Unterberg, J. Phys. Chem. **84** (1980) 3072.
13. A. L. Harris, J. K. Brown and C. B. Harris, Ann. Rev. Phys. Chem. **39** (1988) 341.
14. N. F. Scherer, D. M. Jonas and G. R. Fleming, J. Chem. Phys. **99** (1993) 153.
15. C. Lienau and A. H. Zewail: J. Phys. Chem. **100** (1996) 18629.
16. R. Zadoyan, Z. Li, C. C. Martens and V. A. Apkarian, Chem. Phys. Lett. **218** (1994) 504.
17. D. L. Bunker and B. Slotten Jacobson, J. Am. Chem. Soc. **94** (1972) 1843.
18. J. N. Murrell, A. J. Stace and R. Dammel, J. Chem. Soc. Faraday Trans. 2 **74** (1978) 1532.
19. J. K. Brown, C. B. Harris and J. C. Tully, J. Chem. Phys. **89** (1988) 6687.
20. V. S. Batista and D. F. Coker, J. Chem. Phys. **105** (1996) 4033.
21. H. Hippler, V. Schubert and J. Troe, J. Chem. Phys. **81** (1984) 3931.
22. D. Schwarzer, J. Troe and M. Zerezke, J. Chem. Phys. **107** (1997) 8380.
23. D. Schwarzer, J. Troe and M. Zerezke: J. Phys. Chem. A **102** (1998) 4207.
24. K. L. Saenger, G. M. McClelland and D. R. Herschbach, J. Phys. Chem. **85** (1981) 3333.
25. J. L. Valentini and J. Cross, J. Chem. Phys. **77** (1982) 572.
26. A. Rohrbacher, J. Williams and K. C. Janda, Phys. Chem. Chem. Phys. **1** (1999) 5263.
27. J. A. Beswick, R. Monot, J. M. Philippoz and H. van den Bergh, J. Chem. Phys. **86** (1987) 3965.
28. A. E. Stevens Miller, C.-C. Chuang, H. C. Fu, K. J. Higgins and W. Klemperer, J. Chem. Phys. **111** (1999) 7844.
29. J.-Y. Fang and C. C. Martens, J. Chem. Phys. **105** (1996) 9072.
30. A. J. Conley, J.-Y. Fang and C. C. Martens, Chem. Phys. Lett. **272** (1997) 103.
31. P. S. Dardi and J. S. Dahler, J. Chem. Phys. **93** (1990) 242.
32. P. S. Dardi and J. S. Dahler, J. Chem. Phys. **98** (1993) 363.
33. A. A. Buchachenko and N. F. Stepanov, J. Chem. Phys. **104** (1996) 9913.
34. J. Tellinghuisen, J. Chem. Phys. **82** (1985) 4012.
35. M. W. Balk, C. L. Brooks and S. A. Adelman, J. Chem. Phys. **79** (1983) 804.
36. W. Wang, K. A. Nelson, L. Xiao and D. F. Coker, J. Chem. Phys. **101** (1994) 9663.
37. C. Teichteil and M. Pelissier, Chem. Phys. **180** (1994) 1.